Regulation of shell thickness and shell components in PtCu/PdCu core−shell tripods for ethylene glycol and glycerol oxidation reactions

Houkang Pu[1,†], Kaiyu Dong [1,†], Te Zhang[1], Huizhen Dai[1], Yingying Wang[2,*], Yujia Deng[1,*]

1. School of Chemistry and Chemical Engineering, Qingdao University, Ningxia Road 308, Qingdao 266071, China
2. Qingdao Hengxing University of Science and Technology, Jiushui East Road 588, Qingdao 266100, China

* Correspondence: wangyy_hx@163.com (Y. Wang); dengyujia@qdu.edu.cn (Y. Deng)

† These authors contributed equally to this work.

Experimental Section

Chemicals and Materials

Potassium hexachloroplatinate (IV) (K_2PtCl_6, 98%), sodium tetrachloropalladate (II) (Na_2PdCl_4,98%), Iridium (III) chloride ($IrCl_3$, 99.8%), Sodium iodide (NaI, AR), EG (GC), and glycerol (GC) were procured from Shanghai Macklin Biochemical Co., Ltd. (Shanghai, China). Copper chloride dihydrate ($CuCl_2 \cdot H_2O$, AR) was purchased from Shanghai Yien Chemical Technology Co., Ltd. (Shanghai, China). Tetrachloroauric (III) acid tetrahydrate ($HAuCl_4 \cdot 4H_2O$, AR), poly(vinylpyrrolidone) (PVP, K30), Glycine (AR), L−Ascorbic acid (AA, AR), potassium hydroxide (KOH, AR), and perchloric acid ($HClO_4$, AR) were acquired from Sinopharm Chemical Reagent Co.,

Ltd. (Shanghai, China). Nafion solution (5 wt %) was ordered from Cool chemical science and technology Co., Ltd. (Beijing, China). Ethanol (AR) and acetone (AR) were bought from Tianjin Fuyu Fine Chemical Co., Ltd. (Tianjin, China). Ruthenium (III) chloride anhydrous ($RuCl_3$) was obtained from Shanghai Aladdin Biochemical Technology Co., Ltd. (Shanghai, China). Sodium hexachlororhodate (III) dodecahydrate ($Na_3RhCl_6 \cdot 12H_2O$) was ordered from Thermo Fisher Scientific. All reagents were used as received without further purification, and the water used in all experiments was ultrapure water (18.2 MΩ cm).

Preparation of PtCu TDNs

In the synthesis of PtCu TDNs, 9.8 mg of K_2PtCl_6, 3.4 mg of $CuCl_2 \cdot H_2O$, 400 mg of PVP, 300 mg of NaI, 75 mg of glycine were loaded into a 20 mL polytetrafluoroethylene vessel. Then 7 mL ultrapure water and 1mL EG mixed solution was added. Ultrasonically stirred for 10 min and then loaded into stainless steel autoclave. The reaction kettle was transferred to a muffle furnace, raised from room temperature to 170 °C (6 °C/min), heated for 2 h, and then cooled to room temperature. Typically, we collected the product through centrifugation at 11,000 rpm for 20 min, and then washed twice with ethanol/acetone mixture and ultrapure water. The final product was redispersed in 6 mL of ultrapure water.

Preparation of PtCu/PdCu core−shell TDNs

In the synthesis of PtCu/PdCu core−shell TDNs, 1 mg, 2 mg, 3 mg, 4 mg, 5 mg, 6 mg of Na_2PdCl_4, 60 mg of AA, and 100 mg of PVP were dissolved in 3 mL of ultrapure water and then mixed with 3 mL of the aqueous solution containing PtCu TDNs. After 10 minutes of sonication in the fluoroethylene lining, it was transferred to an autoclave and reacted at 150 °C for 2 h. The product was collected by centrifugation at 11000 rpm for 20 min, and then washed twice with ethanol/acetone mixture and ultrapure water.

Preparation of PtCu/MCu (M= Rh, Ru, Ir, Au) heterostructure TDNs

In the synthesis of PtCu/RhCu heterostructure TDNs, 10.2 mg of $Na_3RhCl_6 \cdot 12H_2O$, 60 mg of AA, and 100 mg of PVP were dissolved in 6 mL of the aqueous solution containing PtCu TDNs. After sonication for 10 min, the reaction was transferred to the autoclave at 150 °C for 2 h. For the preparation of PtCu/AuCu heterostructure TDNs, the precursor was replaced with 500 μL $HAuCl_4$ (48.56 mol/L), and other reaction conditions were unchanged.

In the synthesis of PtCu/RuCu heterostructure TDNs, 4 mg of $RuCl_3$, 60 mg of AA, and 100 mg of PVP were dissolved in 6 mL of EG solution containing PtCu TDNs. After sonication for 10 min, the reaction was transferred to the autoclave at 200 °C for 2 h. For the preparation of PtCu/IrCu heterostructure TDNs, the precursor was replaced with 6 mg of $IrCl_3$ and other reaction conditions were unchanged. The product was collected by centrifugation at 11000 rpm for 20 min, and then washed twice with ethanol/acetone mixture and ultrapure water.

Preparations of PtCu TDNs/C and PtCu/PdCu TDNs/C Catalysts

Disperse the obtained PtCu TDNs and PtCu/PdCu TDNs in 6 mL of ethanol solution containing 3 mg of carbon carrier (Vulcan XC−72), sonicated for 2 h and centrifuged to obtain PtCu TDNs/C and PtCu/PdCu TDNs/C catalyst, washed several times with ethanol/ultrapure water mixed solution and collected by centrifugation. The pretreated catalyst was placed in an N_2/H_2 (5 %) mixture and heat−treated at 250 °C for 1 h. Finally, the sample was dispersed in 950 μL ultrapure water and 50 μL Nafion solution.

Physical characterization

The energy dispersive X−ray spectroscopy (EDS) of PtCu and PtCu/MCu (M=Pd, Rh, Ru) were recorded in a scanning electron microscope (SEM, Hitachi S−4800, Tokyo, Japan). Transmission electron microscope (TEM, JEM−F200, JEOL Ltd, Tokyo, Japan), high−resolution TEM (HRTEM), EDS element mapping, and high−angle circular dark−field scanning TEM (HAADF−STEM) were used to characterize the morphology and structure of PtCu and PtCu/MCu (M=Pd, Rh, Ru, Au) TDNs. The structure and valence state of PtCu and PtCu/PdCu TDNs were analyzed by Bruker D8−Advance (Karlsruhe, Germany) X−ray diffraction (XRD) instrument and X−ray photoelectron spectroscopy (XPS, Thermofisher nexsa). The content of Pt or Pd in the catalysts was determined by inductively coupled plasma atomic emission spectrometry (ICP−AES, 730−ES, Varian).

Electrochemical Measurements

All electrochemical tests were performed on a CHI760E potentiostat (CH Instruments Inc., Shanghai, China). The reference electrode, counter electrode, and working electrode were a saturated calomel electrode, a platinum sheet (1 × 1 cm^2), and a glassy carbon (GC) electrode (3 mm in diameter), respectively. First, the treated PtCu/Pd_{42}Cu TDNs/C, PtCu/Pd_{55}Cu TDNs/C, PtCu/Pd_{77}Cu TDNs/C, PtCu TDNs/C and commercial Pt/C catalysts were dispersed in ultrapure and Nafion (950 μL/50 μL) for 30 min to form homogeneous catalyst inks of 0.122 mg_{Pd}/mL, 0.136 mg_{Pd}/mL, 0.084 mg_{Pd}/mL, 0.363 mg_{Pt}/mL and 0.2 mg_{Pt}/mL, respectively. Catalyst inks of 8 μL were deposited on the surface of the GC electrode and dried naturally. The catalyst−coated working electrode was then placed in 0.1 M $HClO_4$ solution with argon (Ar), and cyclic voltammetry (CV) was performed at the scanning rate of 50 mV/s at the potential range of 0.1 V to 1.05 V vs. RHE to clean the catalyst surface until the curve stabilized. The electrochemically active surface areas (ECSA) of the catalysts were calculated from the charges of the underpotential deposited hydrogen peaks of each catalyst defined as ECSA, while $ECSA_m$ was the result of normalizing ECSA to mass. To determine the EGOR performance of each catalyst, we tested in a 1.0 M KOH + 1.0 M $(CH_2OH)_2$ solution saturated with Ar at a scan rate of 50 mV/s over a potential window of 0.07 ~ 1.37 V vs. RHE. The CV curves of the catalyst in 1.0 M KOH + 1.0 M $C_3H_5(OH)_3$

solution with saturated Ar were recorded at a scan rate of 50 mV/s within the same potential window interval.

DFT calculations

All the density functional theory (DFT) calculations in this work were performed by the Vienna ab initio simulation package (VASP)[1] utilizing the projector augmented wave (PAW) potentials with a plane−wave cutoff energy of 450 eV.[2, 3] The generalized gradient approximation (GGA) functional of Perdew, Burke, and Ernzerhof's (PBE) generalized function applied as the exchange−correlation functional[4] with grime's semiempirical DFT−D3 dispersion correction to describe the van der Waals (vdW) interactions.[5] To prevent the interaction between two adjacent layers, a 15 Å vacuum layer was applied to all surface models. We applied a 3 × 3 × 1 gamma−centered k−point grid to sample the Brillouin zone. The convergence criterion for the electron energy was 10^{-5} eV, and the atomic force for all calculations is 0.03 eV/Å. A 3 × 3 supercell of five layers of Pt (220) facets was constructed. The 13 Pt atoms were then randomly replaced with Cu atoms to satisfy a Pt/Cu ratio of about 7/3 to create the PtCu model. The top two layers of the PtCu model were replaced by Pd and one Cu atom to form the PtCu/PdCu model. The top two layers were relaxed during the optimization process, and the bottom three layers were fixed.

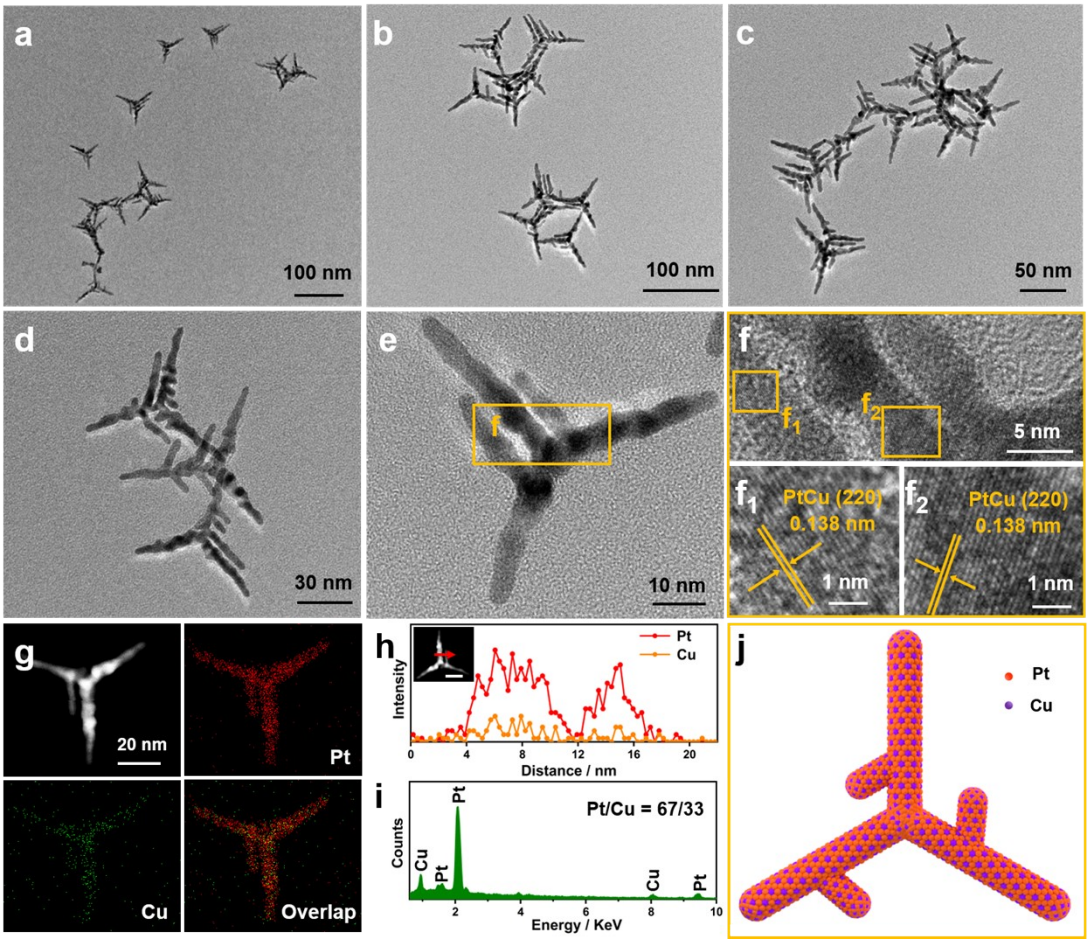

Figure S1. Morphology and structure characterization of PtCu TDNs. (a−e) TEM images of the PtCu TDNs. (f) The HRTEM image of the marked area in Figure S1b. (g) HAADF−STEM image and corresponding STEM−EDS element mapping image of a single PtCu TDN. (h) PtCu TDN scans the image along the element line marked with red. (i) SEM−EDS spectrum of PtCu TNDs. (j) Atomic schematic illustration of the PtCu TDN.

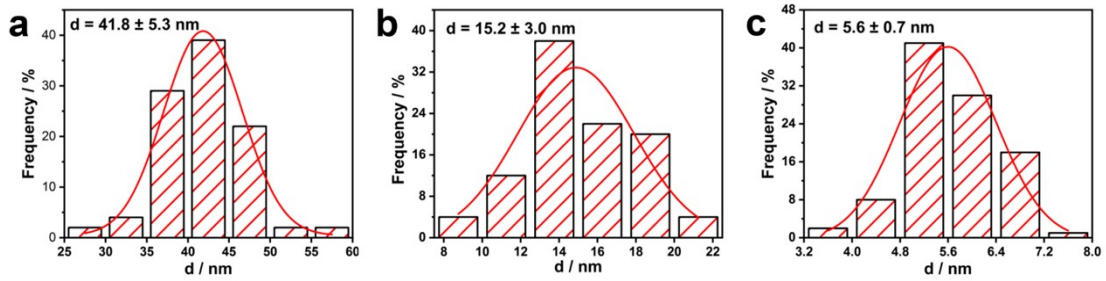

Figure S2. Histograms of the length of the main branch and secondary branch of PtCu TDNs. The width of the main branch of PtCu TDNs.

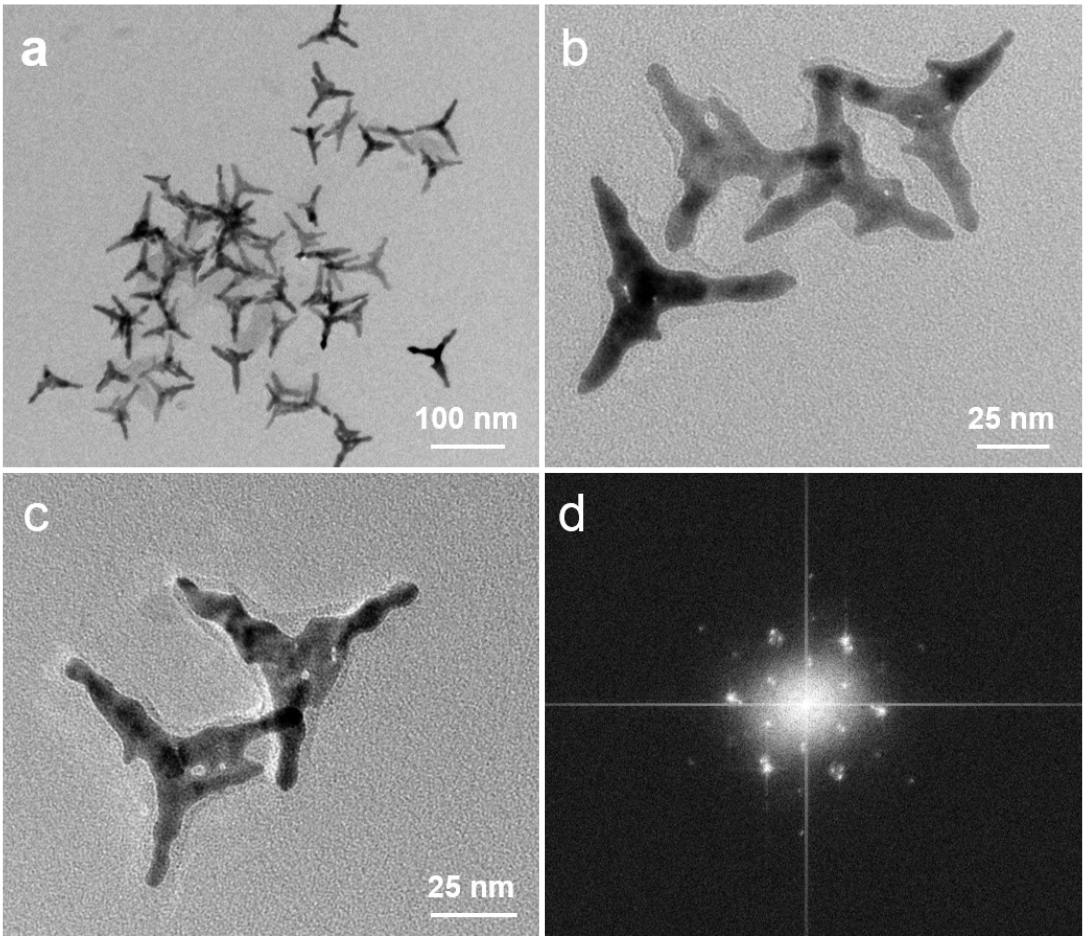

Figure S3. (a−c) TEM images of the PtCu/Pd_{42}Cu TDNs. (d) The corresponding FFT image is in Figure 1c.

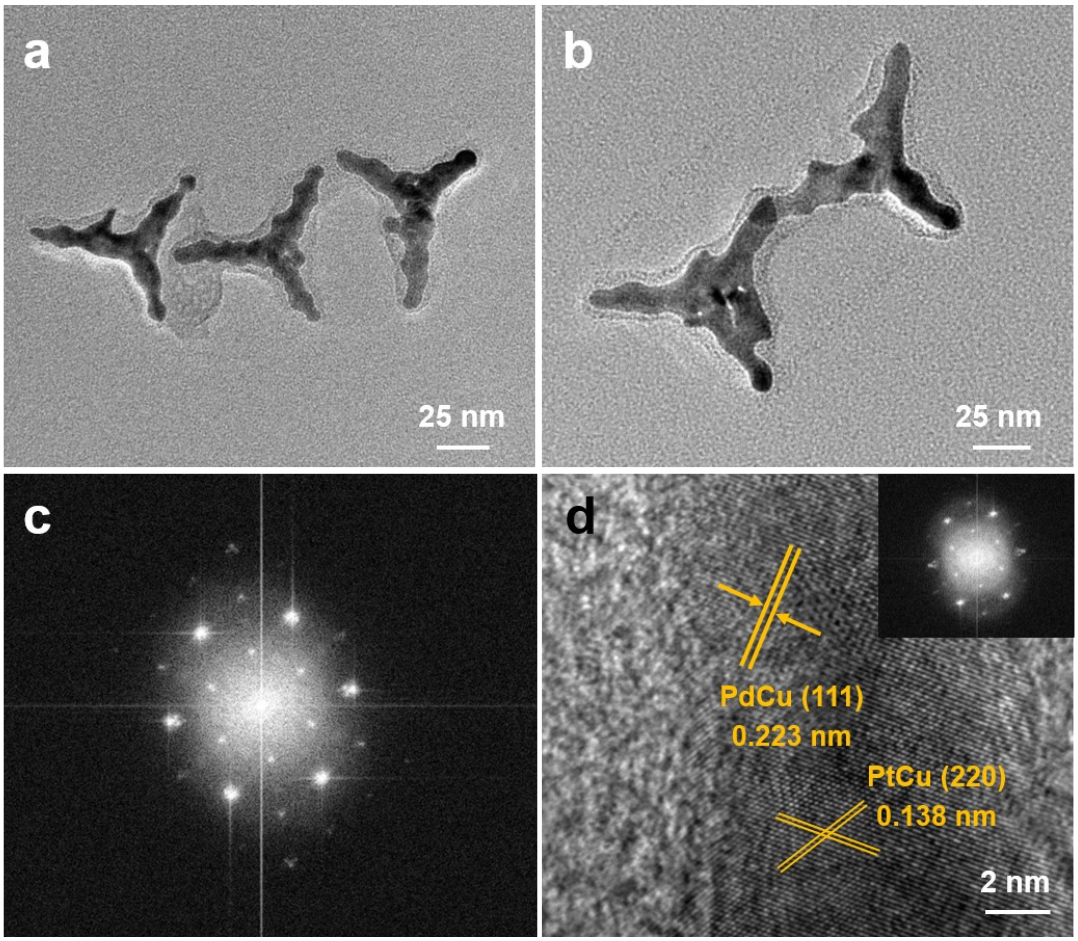

Figure S4. (a−b) TEM images of the PtCu/$Pd_{55}Cu$ TDNs. (c) The corresponding FFT image is in Figure 1i. (d) The HRTEM image of the white marked area in Figure 1h. The illustration shows the corresponding FFT image.

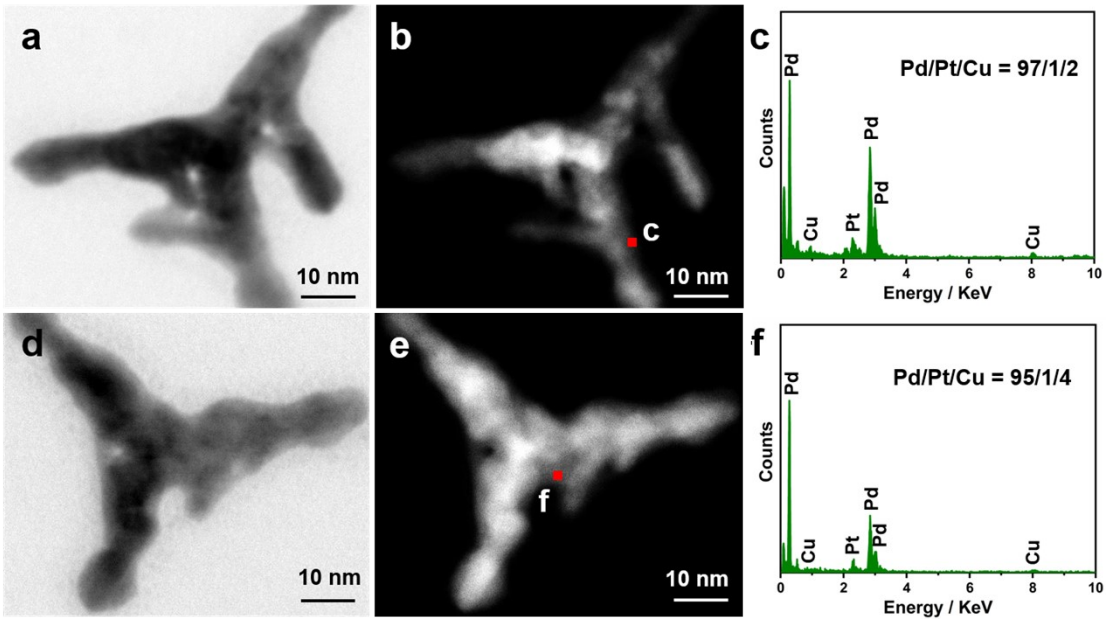

Figure S5. (a−b) and (d−e) The HAADF−STEM image of the PtCu/Pd_{42}Cu and PtCu/Pd_{55}Cu core−shell TDNs. (c) and (f) The STEM−EDS element spot scan image.

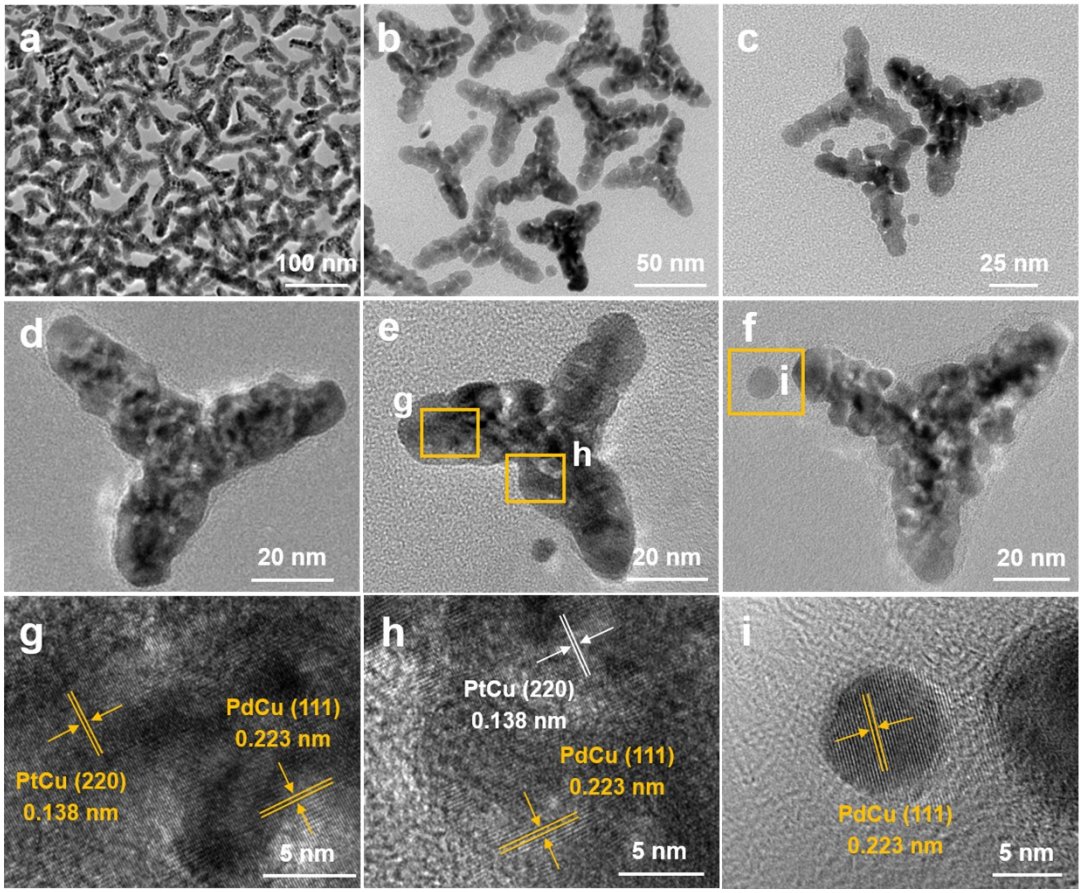

Figure S6. (a−f) TEM images of the PtCu/Pd_{77} TDNs. (g−i) The HRTEM images.

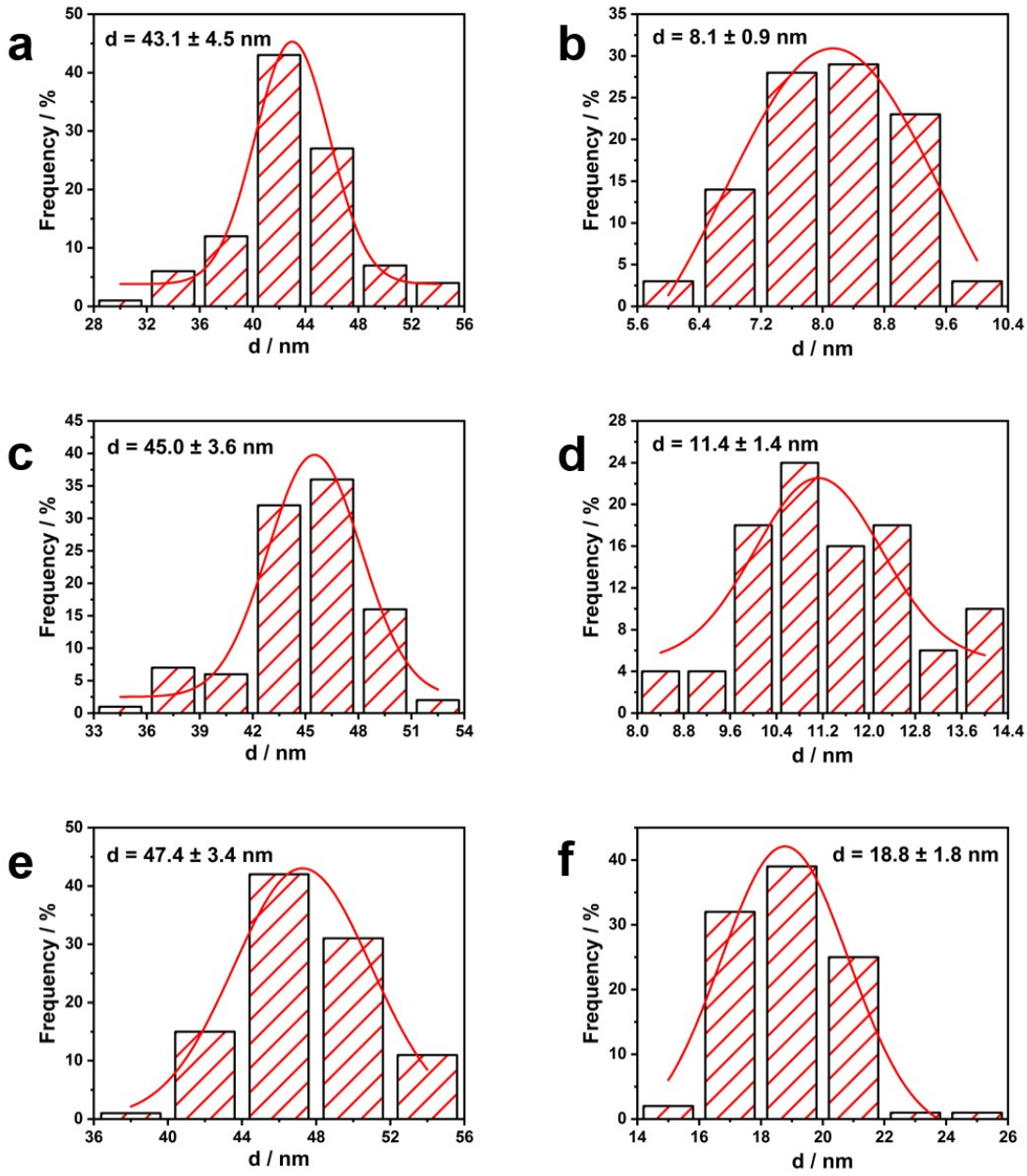

Figure S7. (a), (c) and (e) Histograms of the length of the main branch of PtCu/Pd_{42}Cu, PtCu/Pd_{55}Cu and PtCu/Pd_{77}Cu TDNs, respectively. (b), (d) and (f) Histograms of the width of the main branch of PtCu/Pd_{42}Cu, PtCu/Pd_{55}Cu and PtCu/Pd_{77}Cu TDNs, respectively.

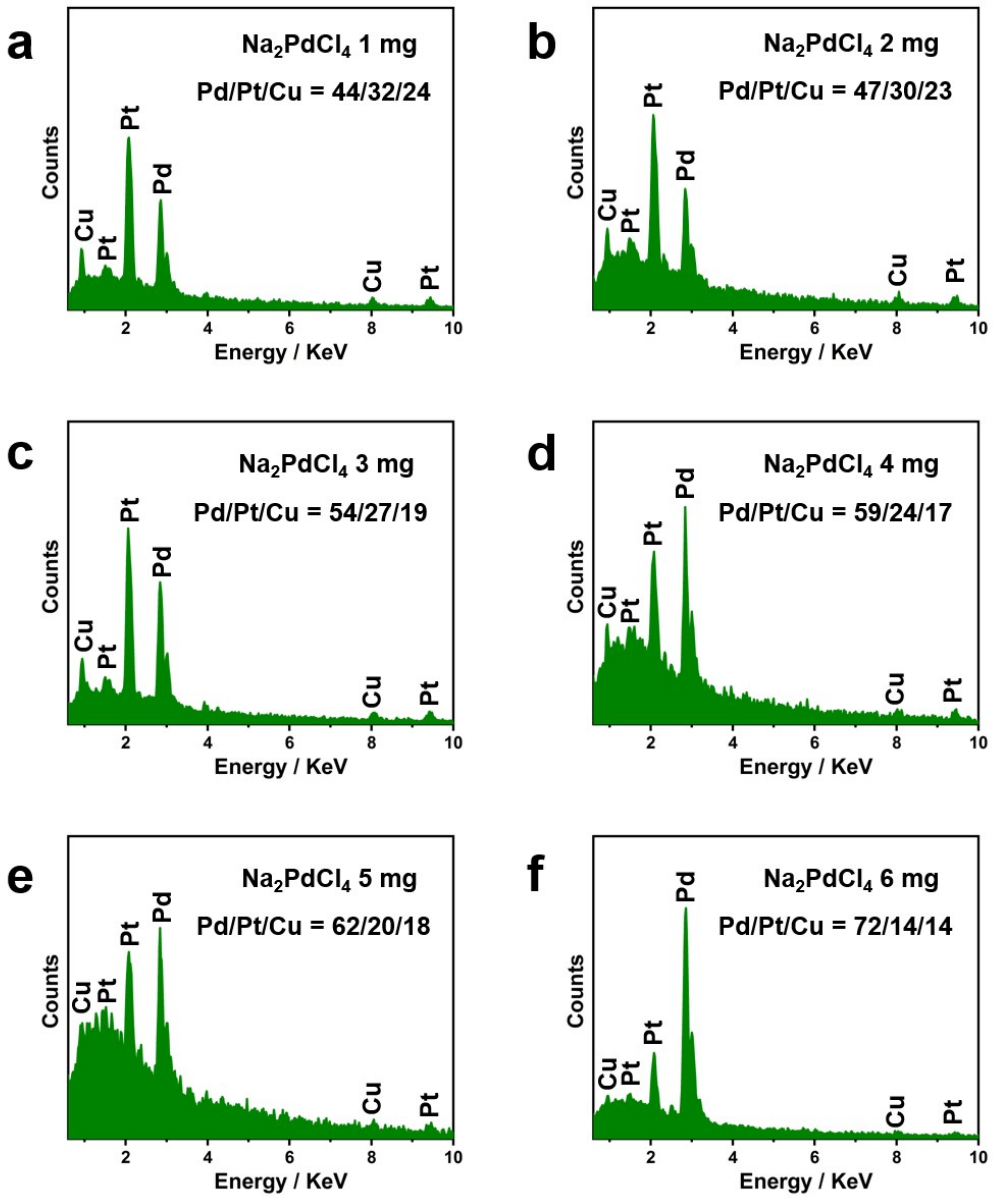

Figure S8. (a−f) SEM−EDS images of products with different Na_2PdCl_4 content.

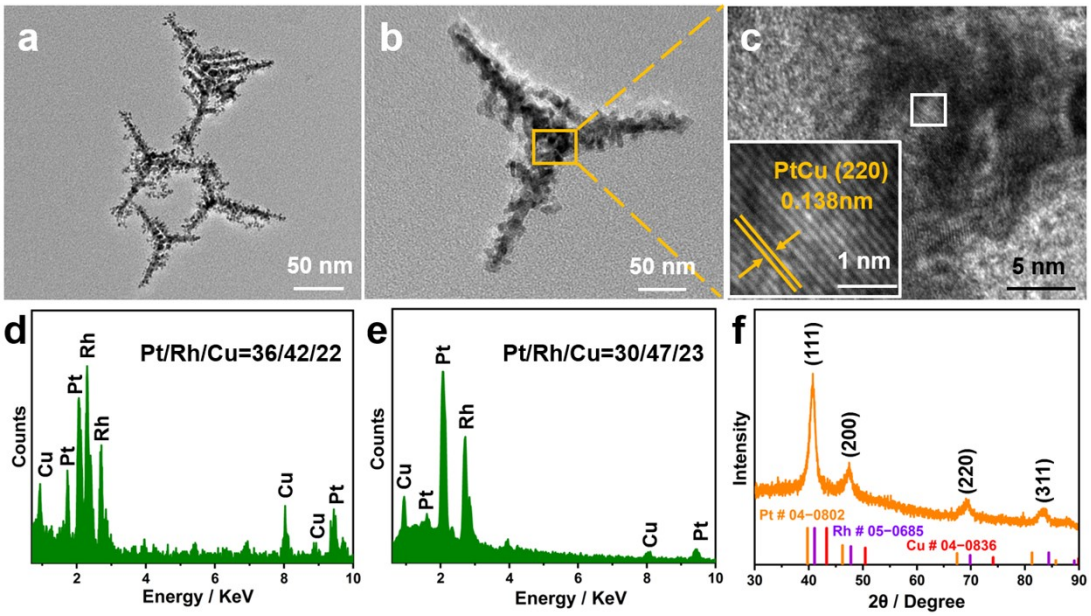

Figure S9. (a−b) TEM images of the PtCu/RhCu heterostructure TDNs. (c) The HRTEM image. The inset shows a magnified image of the marked area in the figure. (d) STEM−EDS elemental mapping spectrum of the PtCu/RhCu heterostructure TDNs. (e) SEM−EDS images of the PtCu/RhCu heterostructure TDNs. (f) PXRD pattern of the PtCu/RhCu heterostructure TDNs.

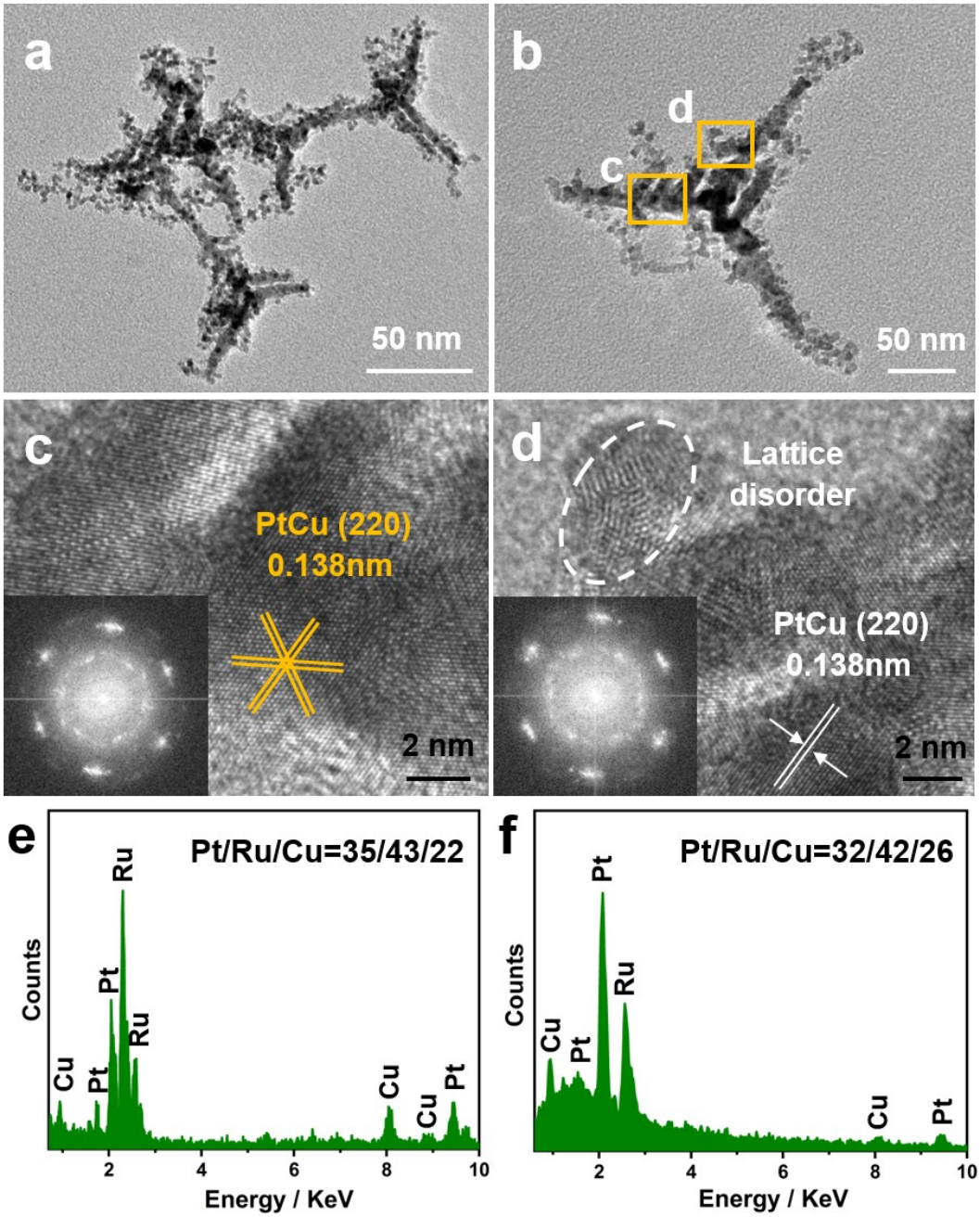

Figure S10. (a−b) TEM images of the PtCu/RuCu heterostructure TDNs. (c−d) The HRTEM images. (e) STEM−EDS elemental mapping spectrum of the PtCu/RuCu heterostructure TDNs. (f) SEM−EDS images of the PtCu/RuCu heterostructure TDNs.

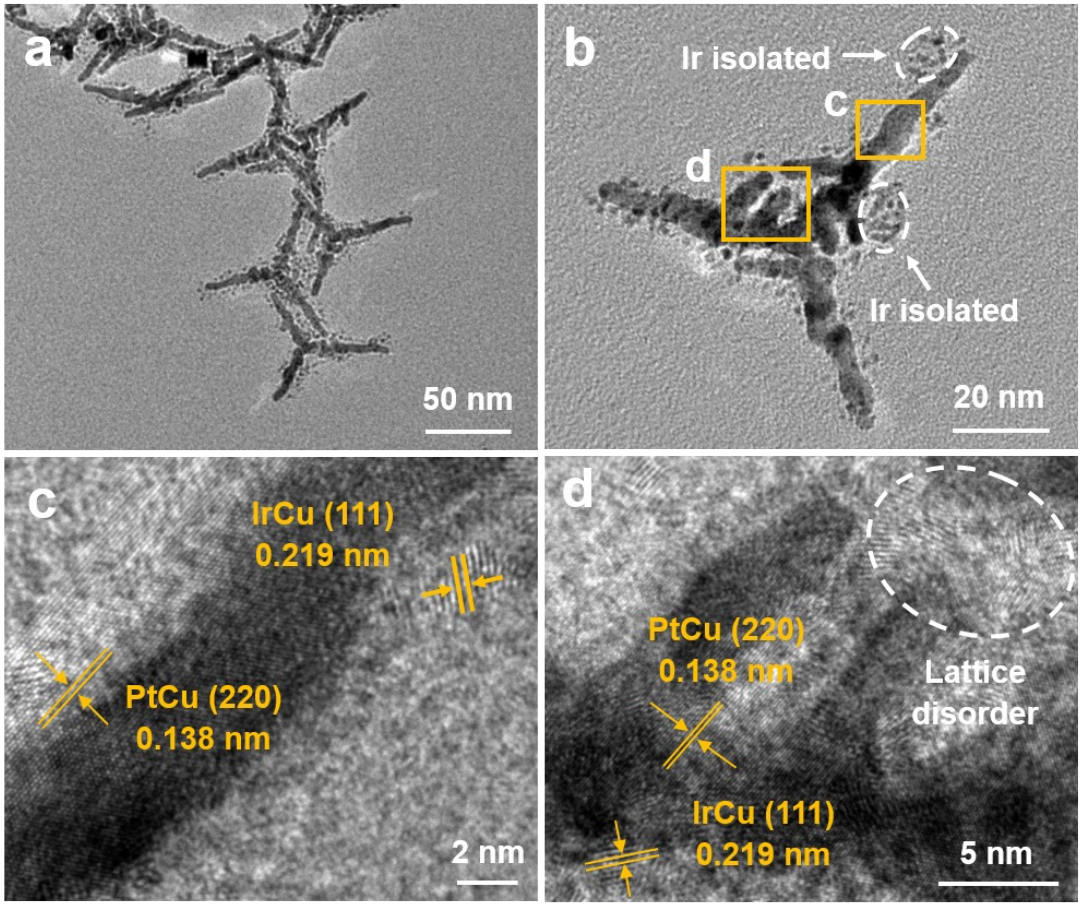

Figure S11. (a−b) TEM images of the PtCu/IrCu heterostructure TDNs. (c−d) The HRTEM images of the corresponding marked area in Figure S10b.

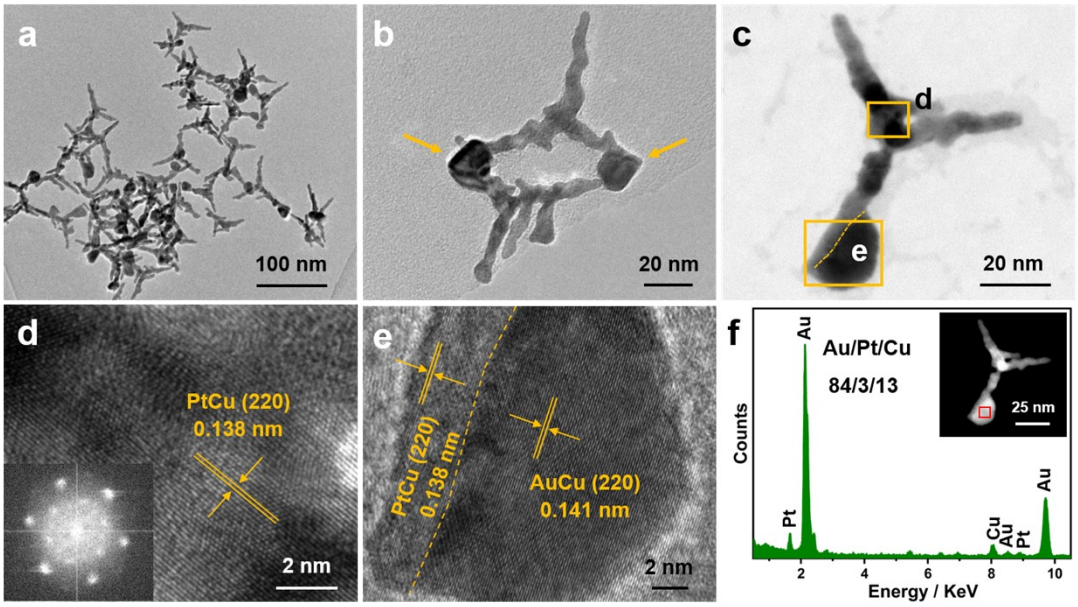

Figure S12. (a−c) TEM images of the PtCu/AuCu heterostructure TDNs. (d−e) The HRTEM image. (f) The STEM−EDS element area scan image for the corresponding marked area.

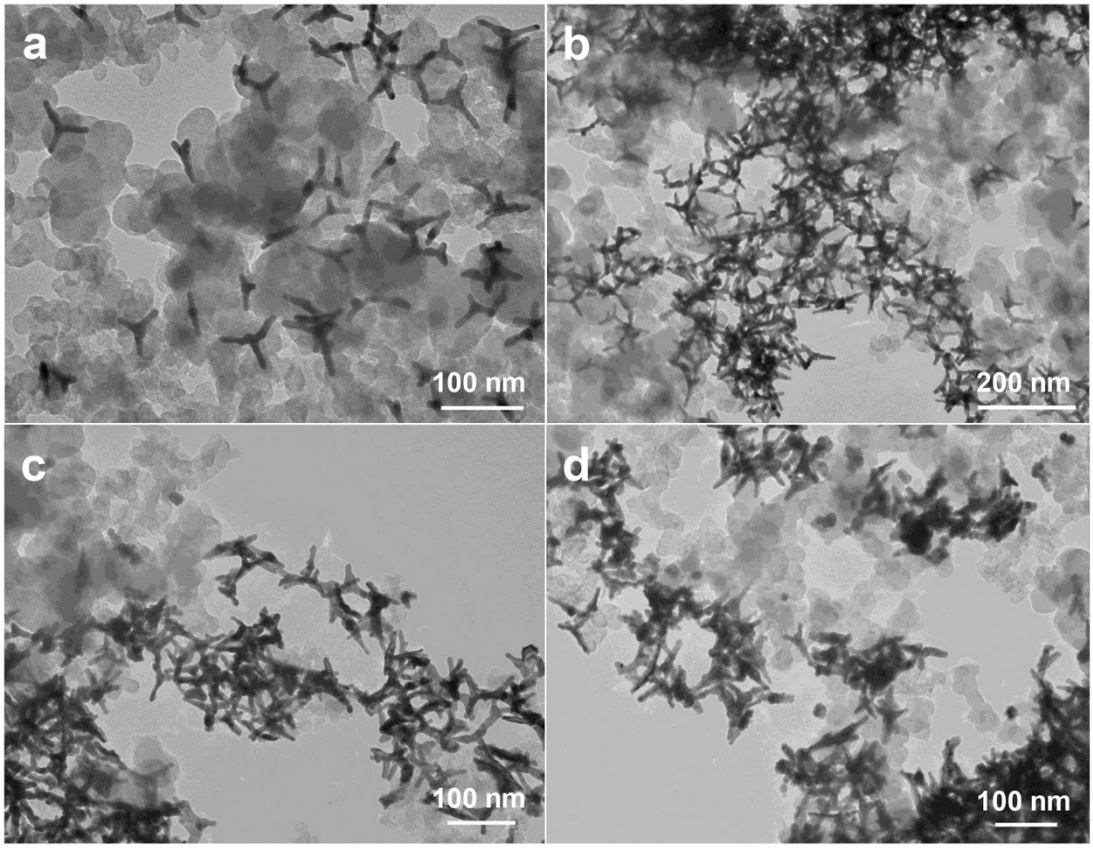

Figure S13. (a−d) TEM images of PtCu TDNs, PtCu/Pd_{42}Cu, PtCu/Pd_{55}Cu, and PtCu/Pd_{77}Cu core−shell TDNs loaded on carbon black, respectively.

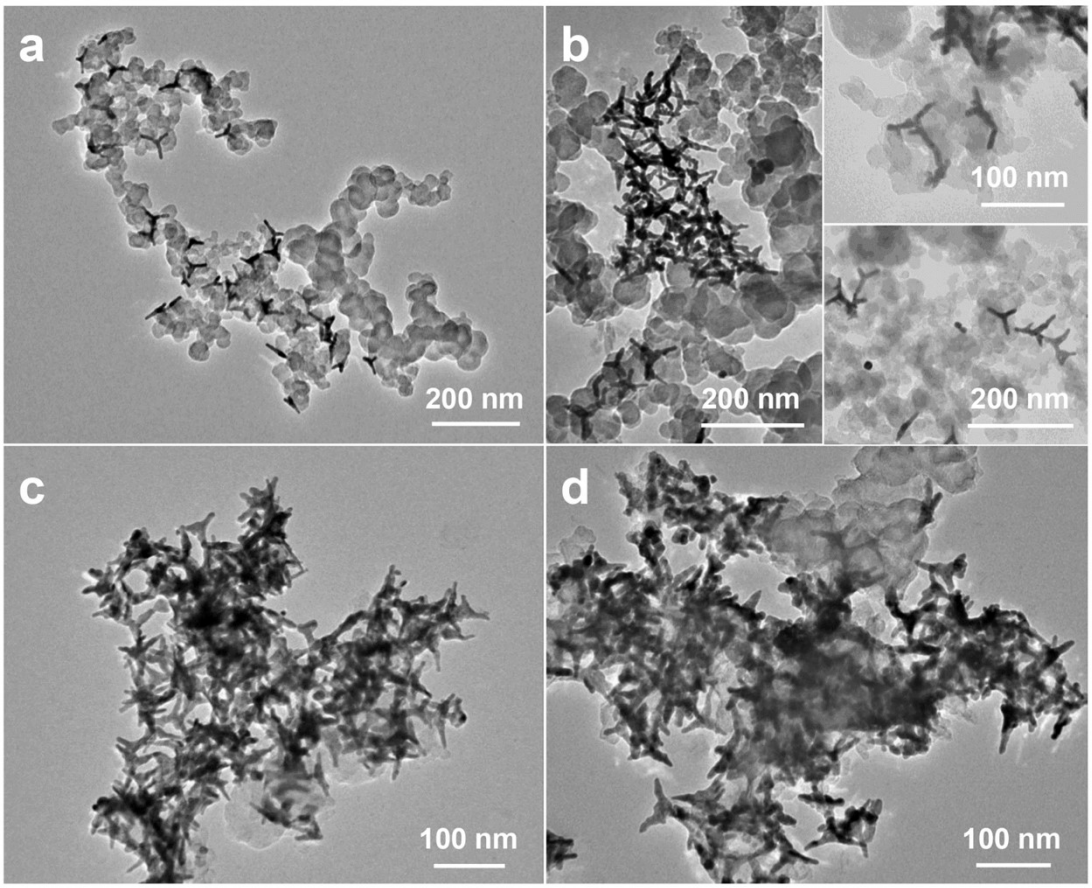

Figure S14. (a−d) TEM images of PtCu TDNs, PtCu/Pd_{42}Cu, PtCu/Pd_{55}Cu, and PtCu/Pd_{77}Cu core−shell TDNs after electrocatalytic test, respectively.

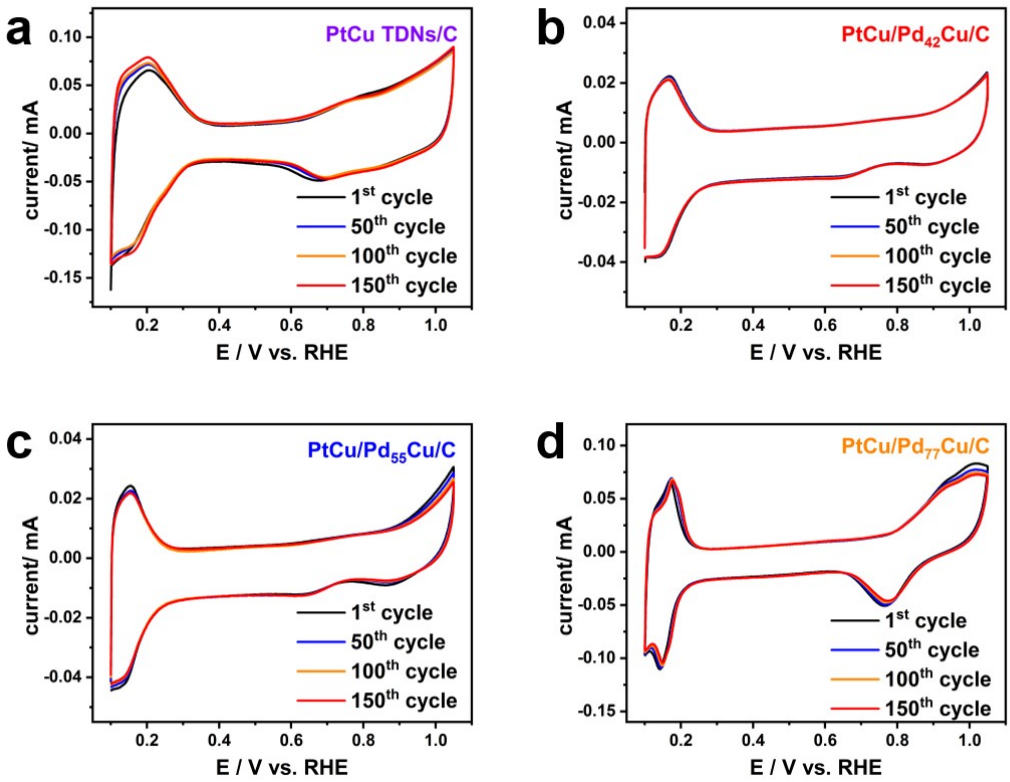

Figure S15. CVs (1st, 50th, 100th and 150th cycle) of (a) the PtCu TDNs/C, (b) $PtCu/Pd_{42}Cu$ TDNs/C, (c) $PtCu/Pd_{55}Cu$ TDNs/C and (d) $PtCu/Pd_{77}Cu$ TDNs/C in an Ar−saturated 0.1 M $HClO_4$ solution at 50 mVs^{-1}, respectively.

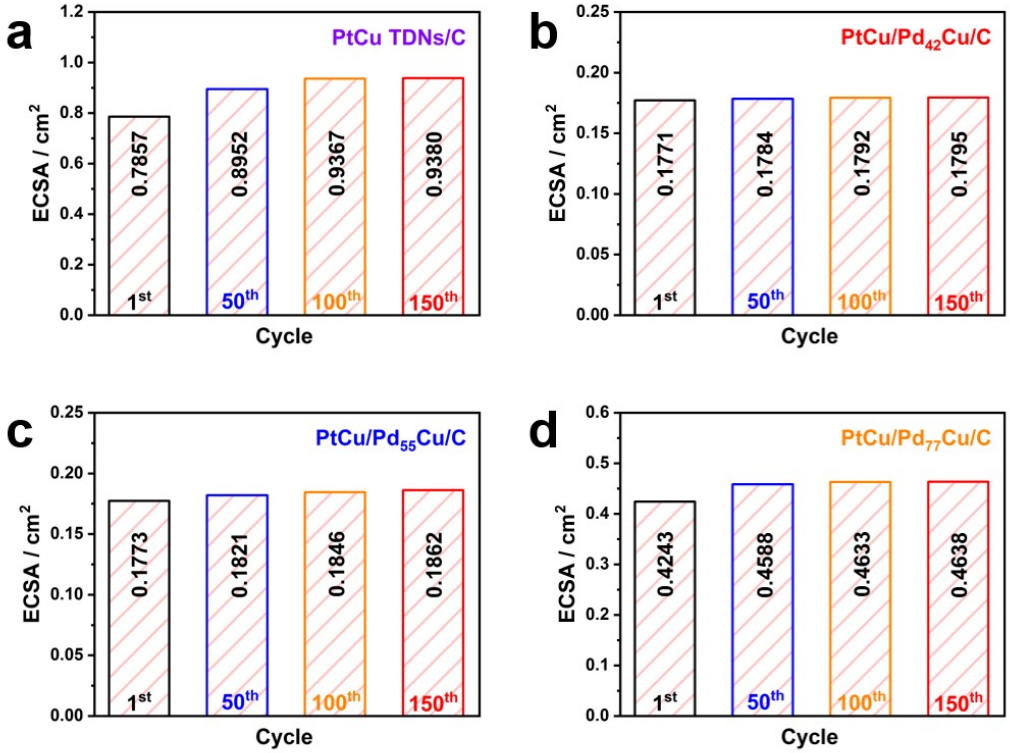

Figure S16. (a−d) Histogram of the trend of ECSA values for PtCu TDNs, PtCu/Pd_{42}Cu TDNs, PtCu/Pd_{55}Cu TDNs, and PtCu/Pd_{77}Cu TDNs, respectively.

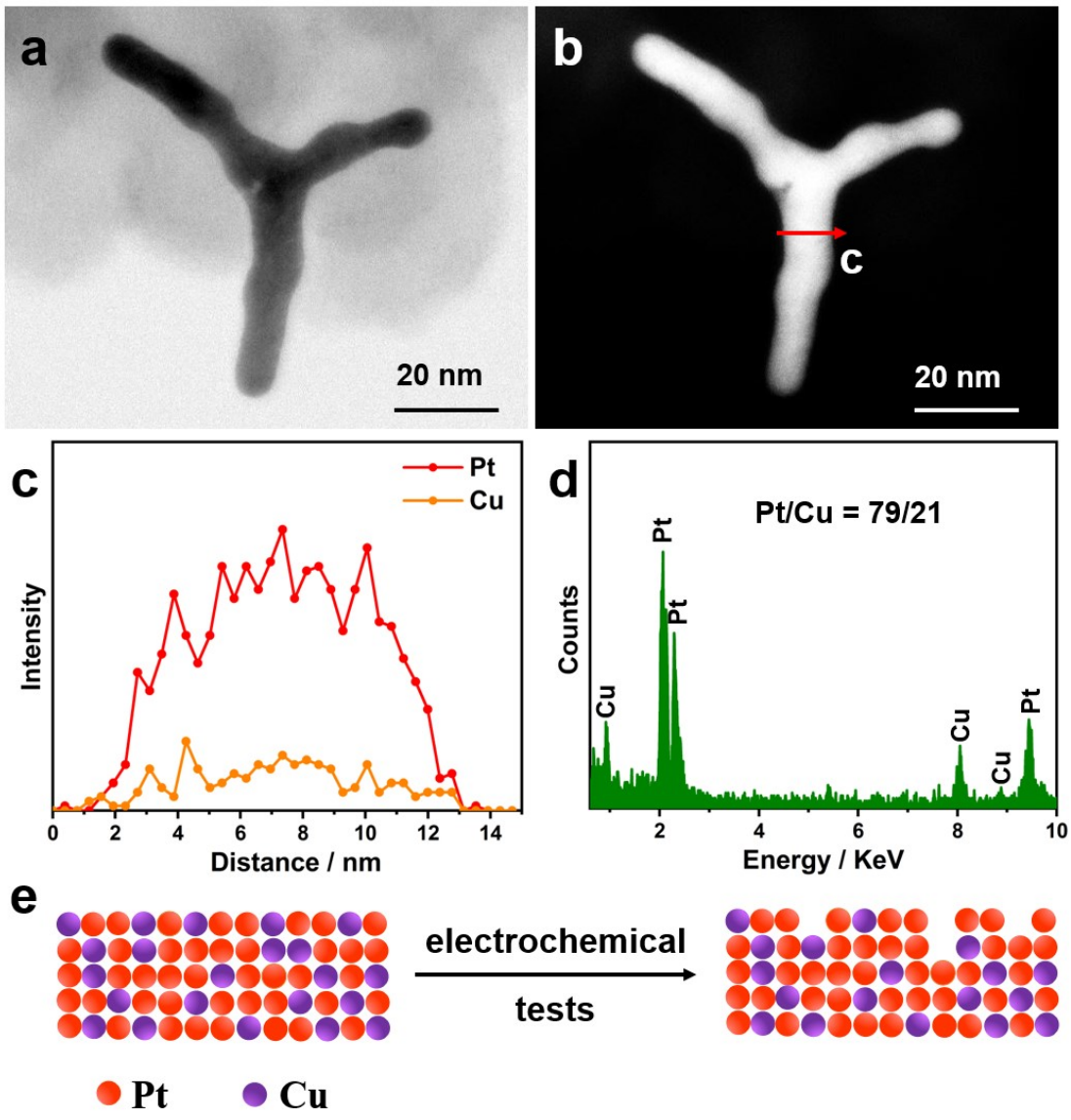

Figure S17. (a−b) The HAADF−STEM image of the PtCu TDNs. (c−d) The STEM-EDS element line scan image and spectrum along the red marking line in figure S16b. (e) Schematic illustrations showed possible changes to the surface composition for PtCu structure during the electrocatalytic testing.

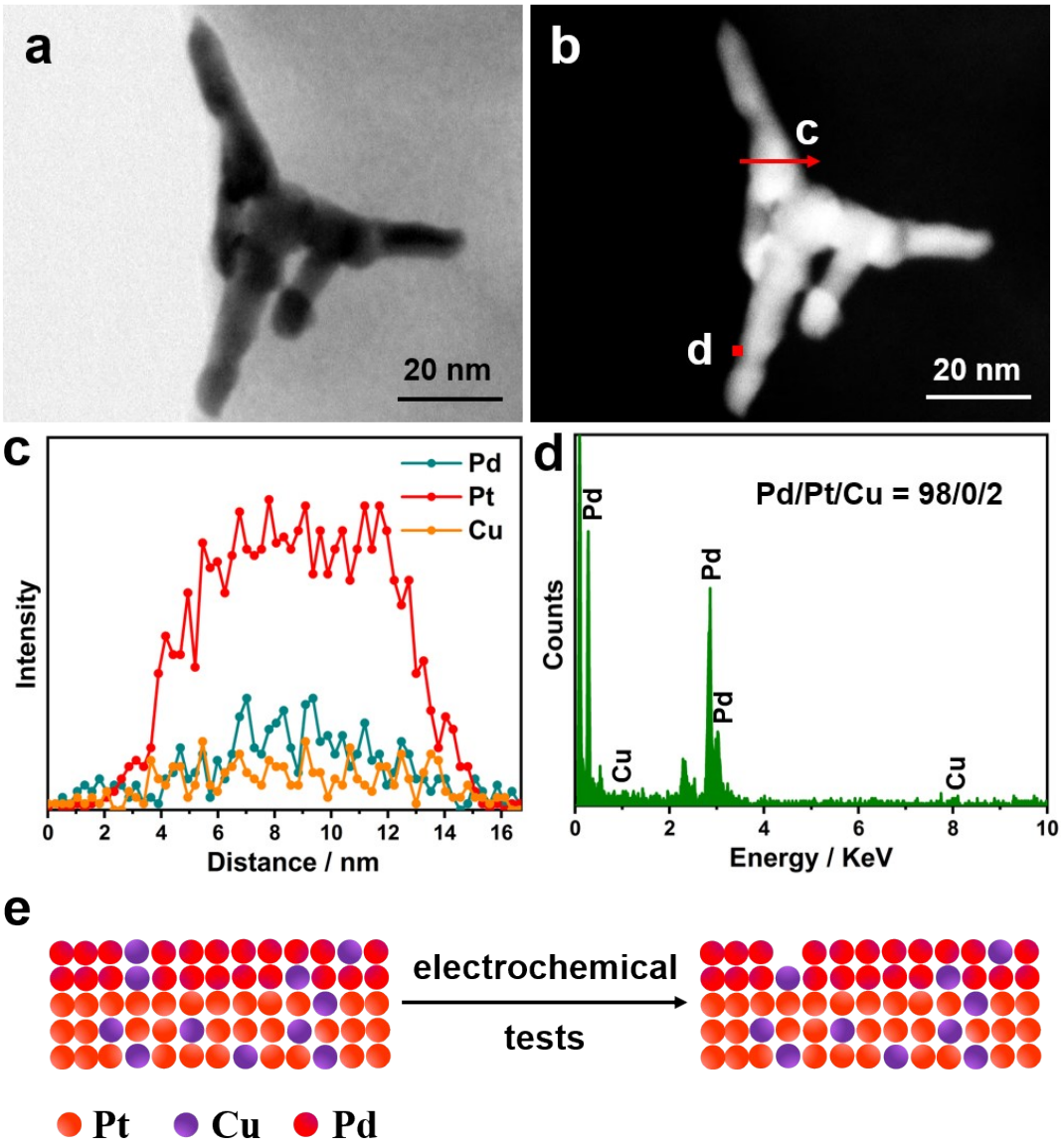

Figure S18. (a–b) The HAADF–STEM image of the PtCu/$Pd_{42}Cu$ TDNs. (c) The STEM-EDS element line scan image. (d) The STEM–EDS element spot scan image. (e) Schematic illustrations showed possible changes to the surface composition for PtCu/$Pd_{42}Cu$ structure during the electrocatalytic testing.

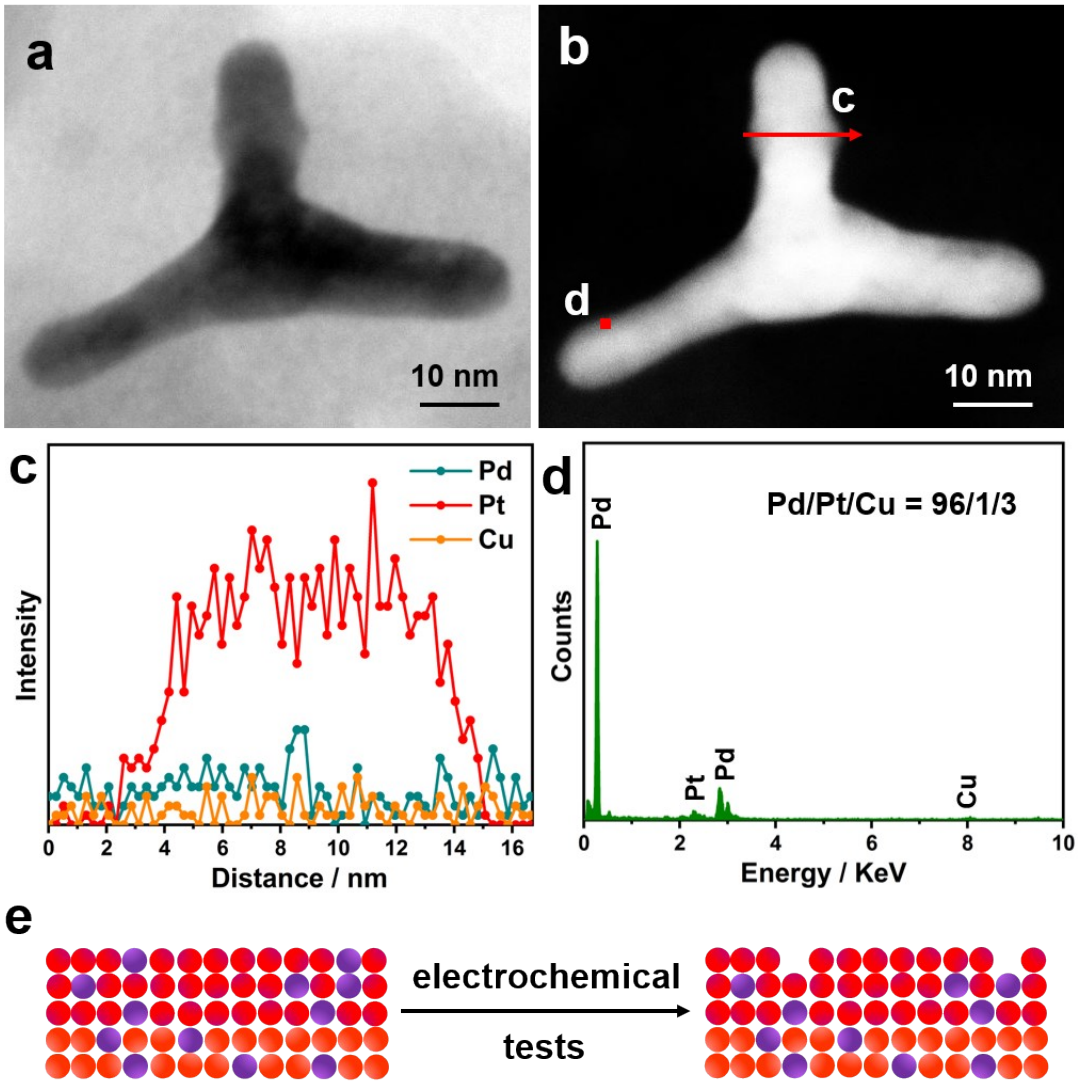

Figure S19. (a−b) The HAADF−STEM image of the PtCu/Pd_{55}Cu TDNs. (c) The STEM-EDS element line scan image. (d) The STEM−EDS element spot scan image. (e) Schematic illustrations showed possible changes to the surface composition for PtCu/Pd_{55}Cu structure during the electrocatalytic testing.

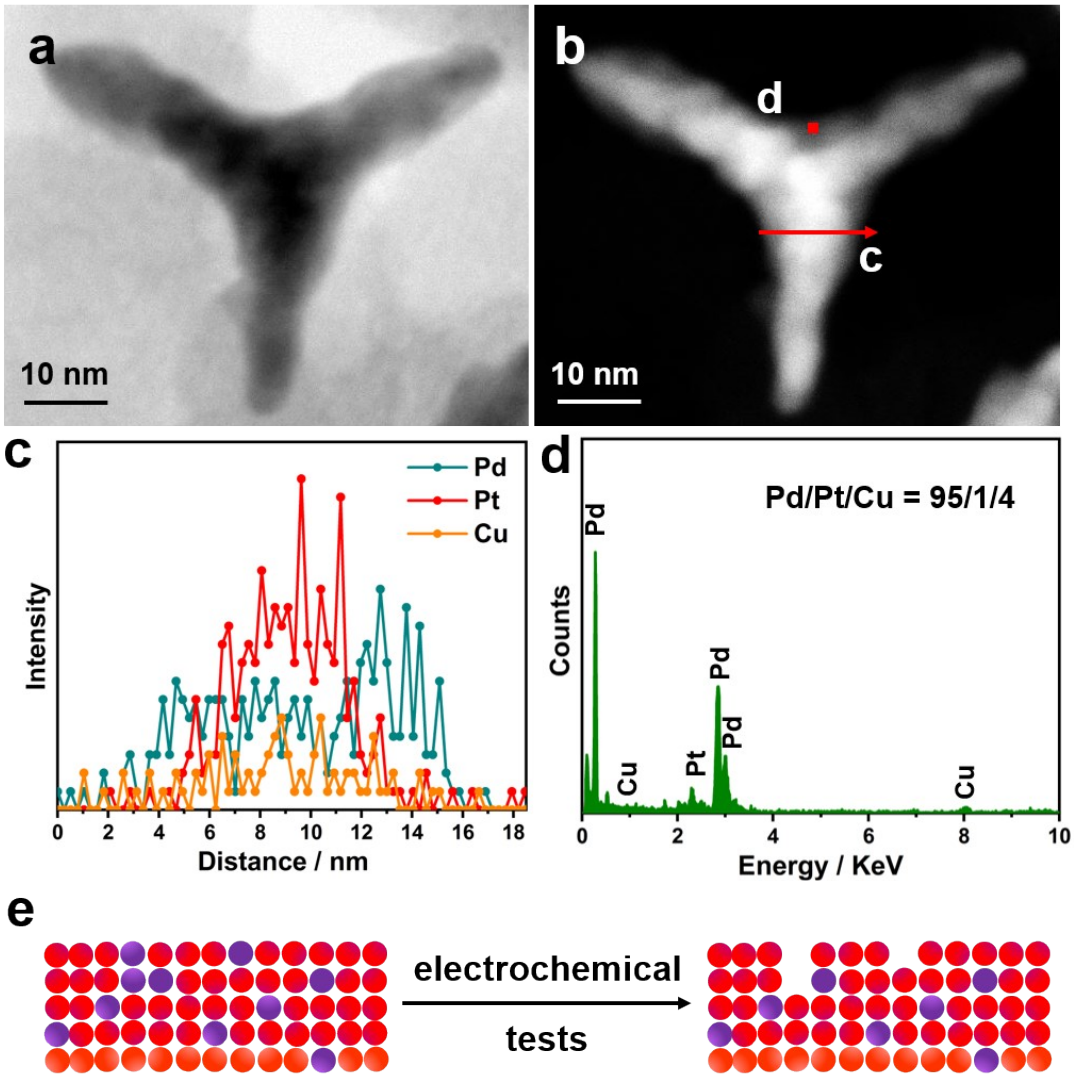

Figure S20. (a–b) The HAADF–STEM image of the PtCu/$Pd_{77}Cu$ TDNs. (c) The STEM–EDS element line scan image. (d) The STEM–EDS element spot scan image. (e) Schematic illustrations showed possible changes to the surface composition for PtCu/$Pd_{77}Cu$ structure during the electrocatalytic testing.

Table S1. EGOR performances of PtCu/$Pd_{42}Cu$ TDNs and various electrocatalysts from published works.

Catalyst	Specific activity /mA·cm^{-2}	Mass activity /A·mg^{-1}	Electrolyte	References
PtCu/$Pd_{42}Cu$ TDNs	72.2	47.0	1.0 M KOH+1.0 M $(CH_2OH)_2$	This Work
THH $Pd_{86.9}Rh_{13.1}$NCs	43.7	–	1.0 M NaOH+1.0 M $(CH_2OH)_2$	6
Pd_2Ag_1	14.8	4.2	1.0 M KOH+1.0 M $(CH_2OH)_2$	7
Pt_4Rh-S NCs	11.6	5.1	1.0 M KOH+1.0 M $(CH_2OH)_2$	8
$Pt_{52}Cu_{48}$ HTNCs	11.2	5.7	1.0 M KOH+1.0 M $(CH_2OH)_2$	9
Pt_3Cu NCs	9.7	5.2	1.0 M KOH+1.0 M $(CH_2OH)_2$	10
Pd_9Ru_1 NSs	9.4	5.9	1.0 M KOH+1.0 M $(CH_2OH)_2$	11
RhCu nanoboxes	1.5	0.8	1.0 M KOH+1.0 M $(CH_2OH)_2$	12
Pd-Ru nanocages	–	5.5	1.0 M KOH+1.0 M $(CH_2OH)_2$	13
$Pd_{58}Cu_{32}Ir_{10}$ NCs	–	4.5	1.0 M KOH+1.0 M $(CH_2OH)_2$	14

Table S2. GOR performances of PtCu/$Pd_{42}Cu$ TDNs and various electrocatalysts from published works.

Catalyst	Specific activity /mA·cm^{-2}	Mass activity /A·mg^{-1}	Electrolyte	References
PtCu/$Pd_{42}Cu$ TDNs	40.8	26.6	1.0 M KOH+1.0 M $C_3H_5(OH)_3$	This Work
$Pt_{89}Co_{11}$ NWs	11.9	4.6	1.0 M KOH+1.0 M $C_3H_5(OH)_3$	[15]
Pd_9Ru_1 NSs	7.0	4.3	1.0 M KOH+1.0 M $C_3H_5(OH)_3$	[11]
$Pt_{52}Cu_{48}$ HTNCs	6.9	3.5	1.0 M KOH+1.0 M $C_3H_5(OH)_3$	[9]
$Pd_{50.2}Cu_{38.4}Pt_{11.4}$	–	9.7	1.0 M KOH+1.0 M $C_3H_5(OH)_3$	[16]
Pd-Ru nanocages	–	6.3	1.0 M KOH+1.0 M $C_3H_5(OH)_3$	[13]
PtCuCo NCs	–	3.5	1.0 M KOH+1.0 M $C_3H_5(OH)_3$	[17]
$Pd_{58}Cu_{32}Ir_{10}$ NCs	–	2.6	1.0 M KOH+1.0 M $C_3H_5(OH)_3$	[14]
Au_1Cu_1	–	2.3	1.0 M KOH+1.0 M $C_3H_5(OH)_3$	[18]

References:

1. G. Kresse and J. Furthmüller, *Physical Review B*, 1996, **54**, 11169-11186.
2. P. E. Blöchl, *Physical Review B*, 1994, **50**, 17953-17979.
3. G. Kresse and D. Joubert, *Physical Review B*, 1999, **59**, 1758-1775.
4. J. P. Perdew, K. Burke and M. Ernzerhof, *Physical Review Letters*, 1996, **77**, 3865-3868.
5. S. Grimme, J. Antony, S. Ehrlich and H. Krieg, *The Journal of Chemical Physics*, 2010, **132**, 154104.
6. J. X. Tang, L. P. Xiao, C. Xiao, N. Tian, Z. Y. Zhou and S. G. Sun, *J Mater Chem A*, 2021, **9**, 11049-11055.
7. F. Gao, Y. P. Zhang, P. P. Song, J. Wang, C. Q. Wang, J. Guo and Y. K. Du, *J Power Sources*, 2019, **418**, 186-192.
8. F. Gao, Y. P. Zhang, P. P. Song, J. Wang, T. X. Song, C. Wang, L. Song, Y. Shiraishi and Y. K. Du, *J Mater Chem A*, 2019, **7**, 7891-7896.
9. H. Xu, P. P. Song, F. Gao, Y. Shiraishi and Y. K. Du, *Nanoscale*, 2018, **10**, 8246-8252.

10. H. Xu, C. F. Liu, P. P. Song, J. Wang, F. Gao, Y. P. Zhang, Y. Shiraishi, J. W. Di and Y. K. Du, *Chem-Asian J*, 2018, **13**, 626-630.
11. B. Zou, F. Gao, H. M. You, Z. L. Li, Y. P. Zhang, Z. Y. Wu, T. X. Song and Y. K. Du, *J Colloid Interf Sci*, 2021, **601**, 42-49.
12. B. Qiao, T. Yang, S. Shi, N. Jia, Y. Chen, X. Chen, Z. An and P. Chen, *Small*, 2021, **17**, 2006534.
13. M. Zhao, Z. Lyu, M. Xie, Z. D. Hood, Z. Cao, M. Chi and Y. Xia, *Small Methods*, 2020, **4**, 1900843.
14. C. Y. Chen, T. X. Song, H. Y. Shang, Q. Y. Liu, M. Y. Yuan, C. Wang and Y. K. Du, *Int J Hydrogen Energ*, 2020, **45**, 26920-26928.
15. Q. W. Sun, F. Gao, Y. P. Zhang, C. Q. Wang, X. Zhu and Y. K. Du, *J Colloid Interf Sci*, 2019, **556**, 441-448.
16. F. Yang, J. Ye, Q. Yuan, X. Yang, Z. Xie, F. Zhao, Z. Zhou, L. Gu and X. Wang, *Adv Funct Mater*, 2020, **30**, 1908235.
17. C. Y. Zhai, J. Y. Hu, H. F. Gao, L. X. Zeng, M. Q. Xue, Z. Q. Liu and M. S. Zhu, *J Taiwan Inst Chem E*, 2018, **93**, 477-484.
18. H. Xu, B. Yan, J. Wang, K. Zhang, S. M. Li, Z. P. Xiong, C. Q. Wang, Y. Shiraishi, Y. Du and P. Yang, *J Mater Chem A*, 2017, **5**, 15932-15939.